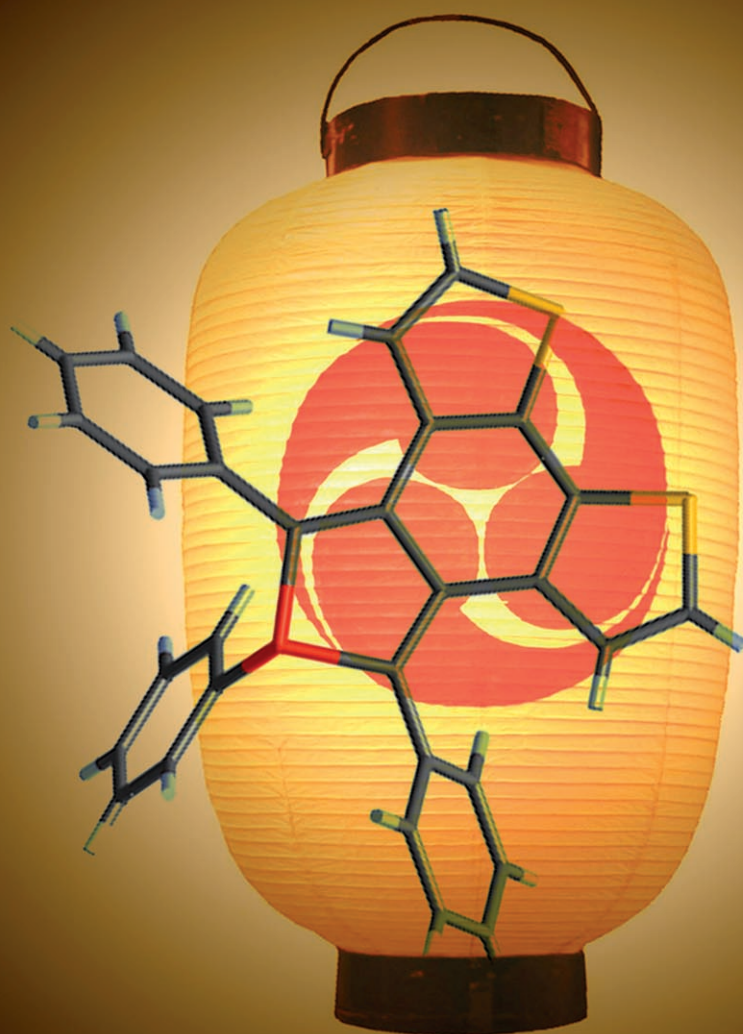# Comparative Study on the Structural, Optical, and Electrochemical Properties of Bithiophene-Fused Benzo[c]phospholes

Yoshihiro Matano,*[a] Tooru Miyajima,[a] Tatsuya Fukushima,[b] Hironori Kaji,[b] Yoshifumi Kimura,[c] and Hiroshi Imahori[a, d, e]

Fusion of Phosphole and Thiophene

Abstract: Three types of bithiophene-fused benzo[c]phospholes were successfully prepared by Ti(II)-mediated cyclization of the corresponding dialkynylated bithiophene derivatives as a key step. Each σ³-phosphorus center of the benzo[c]phosphole subunits was readily transformed into σ⁴-phosphorus center by Au coordination or oxygenation. In addition, the bithiophene subunit was functionalized at the α,α′-carbon atoms by Pd-catalyzed cross-coupling reactions with heteroarylmetals and by an S$_N$Ar reaction with hexafluorobenzene. The experimentally observed results (NMR spectroscopy, X-ray analysis, UV/Vis absorption/fluorescence spectroscopy, and cyclic/differential-pulse voltammetry) have revealed that the structural, optical, and electrochemical properties of the bithiophene-fused benzo[c]phospholes vary considerably depending on the π-conjugation modes at the bithiophene subunits and the substituents of the heterocyclopentadiene components. The appropriately ring-annulated σ³-P derivatives and σ⁴-P-AuCl complexes were found to emit fluorescence in the orange–red region, and the σ⁴-P-oxo derivatives proved to undergo reversible one-electron reduction at −1.4 to −1.8 V (vs ferrocene/ferrocenium). These results indicate that the bithiophene-fused benzo[c]phospholes possess narrow HOMO–LUMO gaps and low-lying LUMOs, which was confirmed by density functional theory calculations of their model compounds. The time-of-flight measurement of an ITO/benzo[c]phosphole/Al device showed that the electron mobility in the P-oxo derivative is one-order higher than that in Alq₃ at low electric fields. The present study demonstrates that the arene-fused benzo[c]phosphole skeleton could be a highly promising platform for the construction of a new class of phosphole-based optoelectrochemical materials.

Keywords: conjugation · fused-ring systems · phosphole · pi interactions · thiophene

Introduction

Heterocyclopentadienes (heteroles) containing the third-row elements such as silicon, phosphorus, and sulfur exhibit characteristic optical and electrochemical properties that originate from the intrinsic nature of their 3s and 3p orbitals. Phosphole, the phosphorus analogue of pyrrole, is a poorly aromatic heterole with a low-lying LUMO due to the effective σ*(P-R)–π*(1,3-diene) orbital interaction.[1] Like other heteroles, phosphole changes its electronic structure by the introduction of π-conjugative substituents at the P-connected *cis*-1,3-diene function. It is worth noting that phosphole is also capable of changing its optical and electrochemical properties by chemical functionalizations (metal coordination, oxygenation, alkylation, etc.) at the phosphorus center. These prominent features of phosphole are beneficial for developing new classes of heterole-based π-conjugated materials for use in optoelectrochemical applications, such as organic light-emitting diodes (OLEDs), field-effect transistors (FETs), and nonlinear optical (NLO) devices.[2] In search of potential candidates for this purpose, much effort has been devoted to reveal the relationship between the structure and the fundamental properties of phospholes bearing π-conjugative substituents at the 2,5-positions (α,α′-positions). For example, Réau and co-workers systematically investigated the optical and electrochemical properties of 2,5-diarylphospholes,[3] and demonstrated the potential utility of this class of compounds as components of the emissive layer for OLEDs.[4] Several other groups have also focused their attention on the light-emitting ability and/or electrochemical properties of oligomers, polymers, and dendrimers incorporating 2,5-diarylphosphole units.[5] Furthermore, phospholes bearing push–pull-type (captodative) π-conjugative substituents at the 2,5-positions were found to behave as potential NLO-phores in solution.[6] Theoretical studies on the phosphole-containing π-conjugated systems have promoted a better understanding of their structure–property relationships.[7]

In addition to the above 2,5-disubstituted systems, ring-fused π-systems, such as dibenzo[b,d]phospholes and dithieno[b,d]phospholes, have been receiving growing interest, as they possess rigid and elongated π-networks that are prerequisite for exhibiting high light-emitting ability.[8,9] In particular, Baumgartner's dithieno[b,d]phospholes have proven to emit intense fluorescence covering the blue–yellow region.[2,9] Quite recently, Yamaguchi and co-workers

[a] Prof. Dr. Y. Matano, T. Miyajima, Prof. Dr. H. Imahori
Department of Molecular Engineering
Graduate School of Engineering, Kyoto University
Nishikyo-ku, Kyoto 615–8510 (Japan)
Fax: (+81) 75-383-2571
E-mail: matano@scl.kyoto-u.ac.jp

[b] T. Fukushima, Prof. Dr. H. Kaji
Institute for Chemical Research
Kyoto University, Uji, Kyoto 611–0011 (Japan)

[c] Prof. Dr. Y. Kimura
Department of Chemistry, Graduate School of Science
Kyoto University, Sakyo-ku, Kyoto 606–8502 (Japan)

[d] Prof. Dr. H. Imahori
Institute for Integrated Cell-Material Sciences (iCeMS)
Kyoto University, Nishikyo-ku, Kyoto 615–8510 (Japan)

[e] Prof. Dr. H. Imahori
Fukui Institute for Fundamental Chemistry
Kyoto University, Takano-Nishihiraki-cho
Sakyo-ku, Kyoto 606–8103 (Japan)

also provided highly emissive bisphosphoryl-bridged stilbenes, the fluorescence quantum yields of which were reported to have reached 99%.[10] Except for these examples, however, the number of ring-fused phosphole-based π-systems is quite limited, and their potential in optoelectrochemical applications has not been fully addressed.

In 2002, Dinadayalane and Sastry reported a theoretical study on the electronic structures and reactivities of a series of unsubstituted benzo[c]heteroles based on density functional theory (DFT) calculations.[11] Taking the calculated HOMO and LUMO energies into consideration, the authors predicted that benzo[c]phosphole would be an attractive platform for the construction of novel phosphole-based π-conjugated systems with a low-lying LUMO and a relatively small HOMO–LUMO gap. Noticeably, the LUMO energy and the HOMO–LUMO gap of benzo[c]phosphole ($E_{LUMO} = -1.97$ eV and $\Delta E_{H-L} = 3.29$ eV calculated at the B3LYP/6–31G* level) are much lower and narrower, respectively, than those of dibenzo[b,d]phospholes ($E_{LUMO} = -0.98$ to -0.97 eV and $\Delta E_{H-L} = 4.94$–4.95 eV calculated at the same level),[12] implying that the position of fused ring(s) dramatically affects the nature of frontier orbitals. Despite this suggestive result, however, the chemistry of benzo[c]phospholes remains unveiled, due to the lack of thermally and kinetically stable derivatives. In other words, the highly reactive *o*-quinonoid character of benzo[c]phosphole has precluded its isolation under ambient conditions.[13] For instance, benzo[c]phospholes with no substituent at the benzo backbone readily undergo Diels–Alder reactions and have not been characterized well.[14] With this in mind, we designed bithiophene-fused benzo[c]phospholes as a new family of benzo[c]phosphole. It was anticipated that the fusion of bithiophene subunit at the benzo backbone would reduce the *o*-quinonoid character and would then bring kinetic and thermal stabilization to the benzo[c]phosphole skeleton. It was also expected that further extension of π-network would be accomplished by chemical functionalizations at the fused bithiophene ring.

Here, we report the first comparative study on the structural, optical, and electrochemical properties of three types of bithiophene-fused benzo[c]phospholes (Figure 1).[15] Both experimental and theoretical results have revealed that the intrinsic nature of the frontier orbitals of the bithiophene-fused benzo[c]phospholes varies significantly depending on the π-conjugation mode of the bithiophene subunits and/or the substituents at the heterole com-
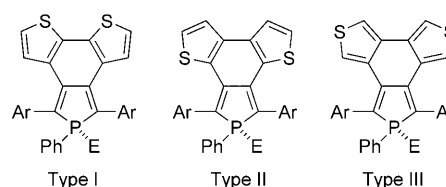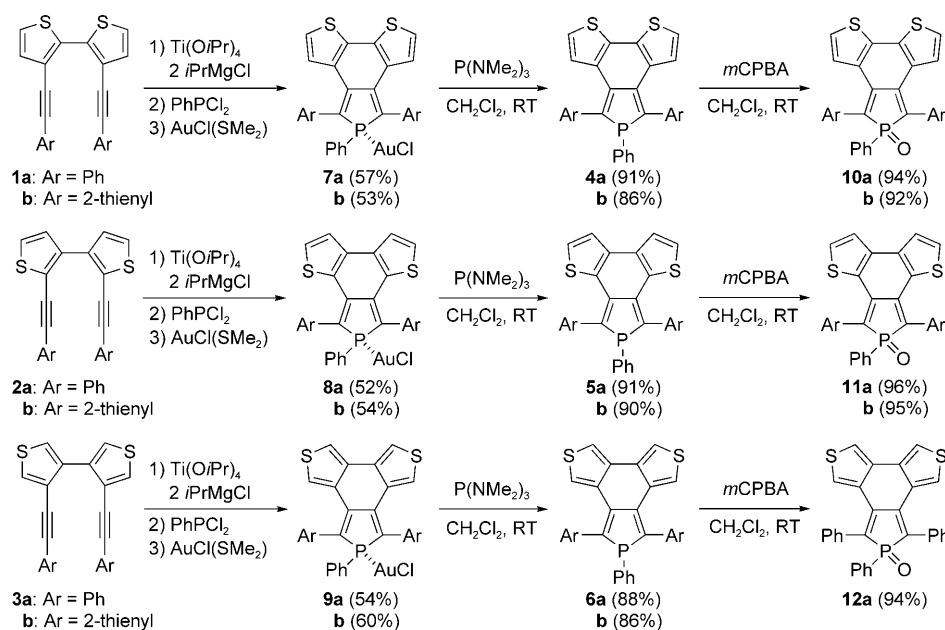

Figure 1. Bithiophene-fused benzo[c]phospholes studied here (E = lone pair, AuCl, O).

ponents. Additionally, we evaluated the electron mobility of a P-oxo derivative by the time-of-flight (TOF) method.

Results and Discussion

Synthesis and characterization of bithiophene-fused benzo[c]phospholes: Bithiophene-fused benzo[c]phospholes **4**–**12** were successfully prepared starting from dialkynylated bithiophene derivatives **1**–**3** as depicted in Scheme 1. The synthesis of the σ³-P derivatives **4**–**6** includes the Ti^{II}-mediated cyclization[16] of diynes **1**–**3** as a key step. Reaction of 3,3′-bis(phenylethynyl)-2,2′-bithiophene (**1a**)[17] with [Ti(OiPr)₂(η²-propene)], generated in situ from [Ti(OiPr)₄] and two equivalents of iPrMgCl,[18] followed by addition of dichloro(phenyl)phosphane, gave a mixture of target compound **4a** and unreacted **1a**, which were not separable by column chromatography. Subsequent treatment of the mixture of **4a** and **1a** with AuCl(SMe₂) selectively converted **4a** to Au^{I}–phosphole complex **7a**, which could be easily separated from **1a** by column chromatography and was isolated as a red solid in 57% yield (based on **1a**). When treated with an excess amount of P(NMe₂)₃ in toluene at room temperature, **7a** readily underwent decomplexation to reproduce the σ³-P

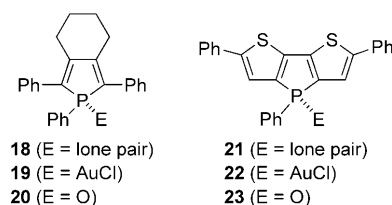Scheme 1. Synthesis of bithiophene-fused benzo[c]phospholes.

derivative **4a** in 91% yield after reprecipitation from MeOH. This two-step protocol enabled us to isolate **4a** in pure form. According to the similar procedures, 2-thienyl-substituted derivatives (**4b** and **7b**) and other two types of bithiophene-fused benzo[c]phospholes (**5, 6, 8,** and **9**) were prepared from the corresponding dialkynylated bithiophene derivatives (**1b, 2a,b,** and **3a,b**). The isolated σ³-P derivatives **4a,b, 5a,b,** and **6a** reacted with m-chloroperbenzoic acid (m-CPBA) at room temperature to give the respective P-oxides **10a,b, 11a,b,** and **12a** in 92–96% yields (Method A; see the Supporting Information). Alternatively, **10–12** were obtained from **1–3** without forming the Au complexes **7–9** (Method B; see the Supporting Information). As illustrated in Figure 1, **4, 7, 10** are classified to the type I, **5, 8, 11** to the type II, and **6, 9, 12** to the type III derivatives.

To investigate substituent effects on the optical and electrochemical properties, we also prepared α,α′-diarylbithiophene-fused benzo[c]phospholes **14–17** starting from the type-I σ³-P compound **4a** (Scheme 2). Treatment of **4a** with an excess amount of n-butyllithium in THF at −78°C, followed by sequential addition of iodine and m-CPBA afforded α,α′-diiodo P-oxo derivative **13** in 40% yield. The Suzuki–Miyaura coupling of **13** with 5-methylthiophen-2-yl-boronic acid in DMF at 110°C produced α,α′-bis(5-methyl-thiophen-2-yl) derivative **14** in 31% yield, whereas the Negishi coupling of **13** with thiazol-2-ylzinc bromide in THF produced α,α′-bis(thiazol-2-yl) derivative **15** in 20% yield. Dilithiated **4a** underwent aromatic nucleophilic substitution (S$_N$Ar) reaction with hexafluorobenzene to afford α,α′-bis-(pentafluorophenyl) σ³-P derivative **16** in 40% yield. The oxygenation of **16** with m-CPBA produced P-oxide **17** in 91% yield.

Compounds **4–17** are air- and thermally stable solids and were fully characterized by conventional spectroscopic techniques (¹H, ¹³C, and ³¹P NMR spectroscopy, MS, and IR

spectroscopy) and elemental analysis. The ¹H NMR spectra of **4–17** in CD₂Cl₂ clearly show C_S symmetry for all the compounds. The α-phenyl ortho-protons of the σ³-P derivatives **4a–6a** were observed equivalently as sharp peaks at room temperature, suggesting that the inversion at the phosphorus center occurs rapidly on the NMR timescale. By contrast, the α-phenyl ortho-protons of the σ⁴-P derivatives **7a–12a** were observed as broad and split peaks at room temperature. The above spectral behavior reflects the difference in hybridization of the phosphorus atom between **7a** and **10a**.

The ³¹P peaks of the σ³-P derivatives **4–6** appeared at δ = 24.2–29.6 ppm, whereas those of Au complexes **7–9** and P-oxides **10–12** appeared at δ = 46.5–51.4 ppm and δ = 35.3–39.5 ppm, respectively. These results support the fact that the phosphorus center is functionalized by Au coordination and oxygenation. The degree of downfield shifts observed for bithiophene-fused benzo[c]phospholes (Δδ = 19.0–23.9 ppm for **7, 8, 9** versus **4, 5, 6**; Δδ = 6.1–13.8 ppm for **10, 11, 12** versus **4, 5, 6**) differs from that reported for 3,4-C₄-methylene-bridged 2,5-diphenylphospholes[3c,4b,5e] (Δδ = 28.1 ppm for **19** versus **18**; Δδ = 30.1 ppm for **20** versus **18**) and α-phenyl-substituted dithieno[b,d]phospholes[9c] (Δδ = 28.7 ppm for **22** versus **21**; Δδ = 39.6 ppm for **23** versus **21**).

18 (E = lone pair)
19 (E = AuCl)
20 (E = O)

21 (E = lone pair)
22 (E = AuCl)
23 (E = O)

Apparently, the P-substituent effect on the chemical shift is related to the π-conjugated framework at the phosphole
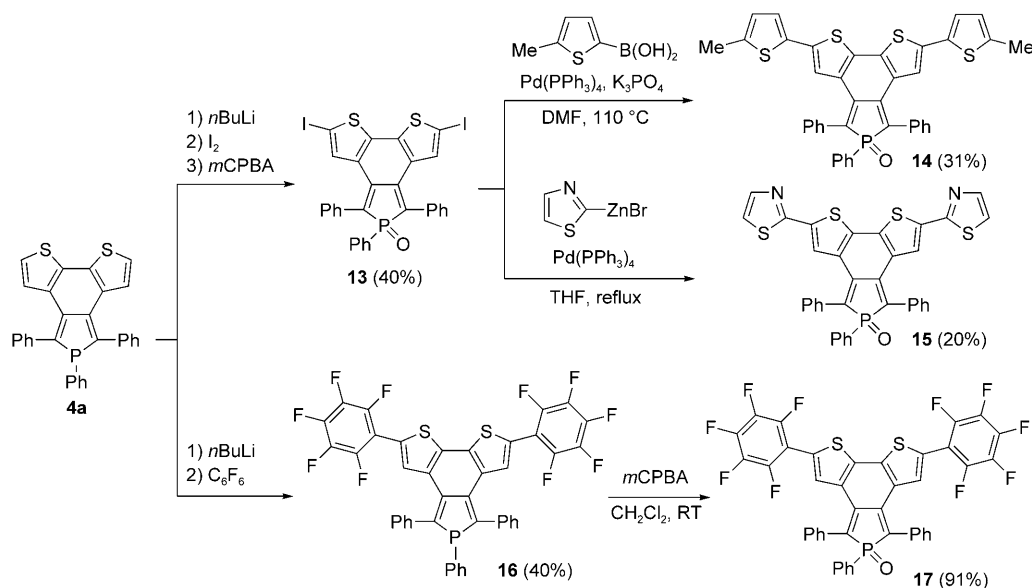
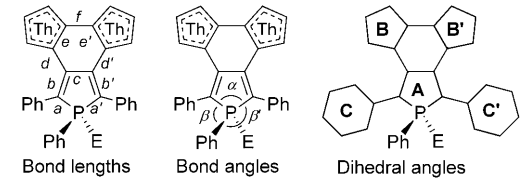Scheme 2. Functionalization of bithiophene-fused benzo[c]phospholes.

ring. The ^{31}P peaks of the σ^3-P derivative **16** ($\delta = 26.3$ ppm) and the P-oxo derivatives **13–15** and **17** ($\delta = 37.3$–37.9 ppm) are close to the respective ^{31}P chemical shifts of **4a** ($\delta = 24.6$ ppm) and **10a** ($\delta = 37.8$ ppm). It seems that the α,α'-substituents of the fused bithiophene subunit do not affect the electronic character at the phosphorus center significantly. The IR spectra of the P-oxides **10–15** and **17** showed characteristic P–O stretching bands at $\nu_{max} = 1187$–1200 cm^{-1}.

Crystal structures of bithiophene-fused benzo[c]phospholes: The crystal structures of **4a**, **5a**, and **7a–10a** were unambiguously elucidated by X-ray diffraction analyses. Single crystals were grown from CH$_2$Cl$_2$–MeOH (for **4a**, **5a**, **7a–9a**) or CH$_2$Cl$_2$–hexane (for **10a**) at room temperature. The ORTEP diagrams are depicted in Figure 2, packing structures are shown in Figure S1 in the Supporting Information, selected bond lengths, bond angles, and dihedral angles are listed in Table 1, and crystallographic parameters are summarized in Table 3 in the Experimental Section.[19] Each phosphorus center in the σ^3-P derivatives **4a** and **5a** is pyramidalized with the sum of C-P-C bond angles ($\Sigma_{C\text{-}P\text{-}C}$) of 299.5–303.2°, whereas that in the σ^4-P derivatives **7a–10a** adopts a distorted tetrahedral geometry with $\Sigma_{C\text{-}P\text{-}C}$ of 306.1–310.9°. The π-conjugated phosphole and bithiophene rings are nearly on the same plane with dihedral angles (**A–B** and **A–B'**; Table 1) of 1.5–10.6°. For all the compounds, the phosphorus atom is slightly deviated by 0.05–0.28 Å from a cyclic 1,3-diene plane of the phosphole ring. The C–C/C=C bond length alternation observed for the benzo[c]phosphole skeleton (b–f in Table 1) is little affected by the P functionalization, suggesting that the P lone pair in the σ^3-P derivatives hardly mixes into the 1,3-dienic π-system of the phosphole ring. The bonds at e/e' of **9a** are longer by 0.06–0.07 Å than those of **7a** and **8a**, and the carbon–carbon bonds making the central six-membered ring (c, d/d', e/e', and f) of **9a** have considerable single-bond character. These data clearly exhibit the difference in the π-conjugation mode of bithiophene subunits; the benzo[c]phosphole character of the

Table 1. Selected bond lengths, bond angles, and dihedral angles of **4a**, **5a**, and **7a–10a**.

	4a	**5a**	**7a**	**8a**[a]	**9a**[a]	**10a**
E	–	–	AuCl	AuCl	AuCl	O
bond lengths [Å]						
a	1.796(2)	1.801(2)	1.792(4)	1.802(6)	1.793(8)	1.800(5)
a'	1.793(2)	1.805(2)	1.787(4)	1.787(6)	1.795(8)	1.806(5)
b	1.374(2)	1.365(3)	1.353(6)	1.360(8)	1.359(11)	1.359(6)
b'	1.374(2)	1.366(3)	1.373(6)	1.367(8)	1.351(11)	1.358(6)
c	1.486(2)	1.491(3)	1.502(6)	1.495(8)	1.499(11)	1.505(6)
d	1.461(2)	1.446(3)	1.453(6)	1.459(8)	1.465(11)	1.469(6)
d'	1.461(2)	1.453(3)	1.457(6)	1.445(8)	1.470(11)	1.485(6)
e	1.386(2)	1.383(3)	1.368(6)	1.379(8)	1.437(11)	1.392(6)
e'	1.385(2)	1.378(3)	1.389(6)	1.383(8)	1.445(11)	1.385(6)
f	1.424(2)	1.454(3)	1.436(7)	1.452(8)	1.442(11)	1.416(6)
bond angles [°]						
α	92.22(7)	91.85(1)	94.1(2)	94.3(3)	93.6(4)	93.6(4)
β	106.00(7)	103.14(1)	106.9(2)	106.5(2)	104.8(4)	107.7(4)
β'	104.96(7)	104.46(1)	109.9(2)	108.6(3)	107.7(4)	104.8(4)
dihedral angles [°][b]						
A–B	6.0	1.6	3.3	9.5	10.6	3.0
A–B'	8.8	1.5	7.7	2.6	2.8	5.5
A–C	53.1	82.9	88.0	61.5	64.7	83.7
A–C'	54.7	81.9	51.8	80.4	76.7	62.3

[a] Data of one of the pairing molecules. [b] Dihedral angles between the mean planes **A** and **B/B'/C/C'**.

type-III derivatives should be very weak as compared to that of the type-I and type-II derivatives. Among the type-I derivatives, the C$_\alpha$–C$_\beta$ and C$_\beta$–C$_\beta$ bond lengths in the phosphole ring of **4a** ($b/b' = 1.374(2)$ Å; $c = 1.486(2)$ Å) differ only slightly from those of **7a** ($b/b' = 1.353(6)$-1.373(6) Å; $c = 1.502(6)$ Å) and **10a** ($b/b' = 1.358(6)$-1.359(6) Å; $c = 1.505(6)$ Å). The packing structures of the present P,S-hybrid π-systems definitely depend on hybridization at the phosphorus center: the σ^3-P derivative **4a** adopts head-to-tail orientation, whereas the σ^4-P-Au complex **7a** adopts head-to-head orientation (Figure S1 in the Supporting Information). The Au–P bond lengths (2.2198(15)–2.2283(10) Å) and the P-Au-Cl bond angles (175.17(6)–177.57(9)°) of **7a–9a** are within the range of typical values of known Au–phosphole complexes, including **19** and **22**.[20] In contrast to the previously reported Au complexes, however, there is no Au–Au interaction in the packing structures of **7a–9a**, which adopt head-to-head orientation with a par-
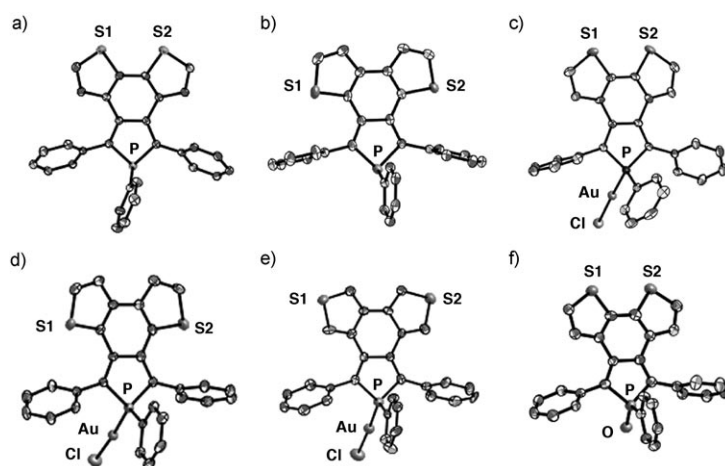

Figure 2. The ORTEP diagrams (50% probability ellipsoids) of a) **4a**, b) **5a**, c) **7a**, d) **8a**, e) **9a**, and f) **10a**.

allel π–π stacking motif (**7a**) or a twisted π–π stacking motif (**8a** and **9a**) as shown in Figure S1 in the Supporting Information.[21] It is likely that steric congestion around the phosphorus center directs the head-to-head orientation of the present Au complexes.[22] In all the compounds characterized, two benzene rings attached to the α-positions are twisted significantly out of the phosphole ring plane with torsion angles (**A–C** and **A–C′**) of 53.1–88.0°. This may be partly due to packing effects derived from the close proximity of the two hybrid π-systems.

Optical properties of bithiophene-fused benzo[c]phospholes: Compounds **4–17** are yellow, orange, or purple solids soluble in CHCl$_3$, CH$_2$Cl$_2$, THF, and toluene. To disclose the optical properties of a series of bithiophene-fused benzo[c]-phospholes, we measured UV/Vis absorption and fluorescence spectra of **4–17** in CH$_2$Cl$_2$ (Table 2, Figure 3, and Figure S2 in the Supporting Information). The absorption spectra of the phenyl-substituted derivatives **4a** and **5a** display broad π–π* transitions at around 400–550 nm, and the fluorescence spectra of **4a** and **5a** show broad emissions in the orange region (500–800 nm) with fluorescence quantum yields (Φ_F) of 17.6% and 9.7%, respectively. The absorption and fluorescence maxima of **4a** ($\lambda_{abs}=462$ nm; $\lambda_{em}=600$ nm) and **5a** ($\lambda_{abs}=472$ nm; $\lambda_{em}=609$ nm) are largely red-shifted relative to those of **18** ($\lambda_{abs}=354$ nm; $\lambda_{em}=466$ nm)[3c] and **21** ($\lambda_{abs}=431$ nm; $\lambda_{em}=470$ nm),[9c] which represents the effective π-extension in the present P,S-hybrid π-systems of types I and II. In marked contrast to **4a** and **5a**, the type-III compound **6a** displays weak absorption and emission bands at $\lambda_{abs}=395$ nm (shoulder) and $\lambda_{em}=548$ nm ($\Phi_F=0.6$%). A
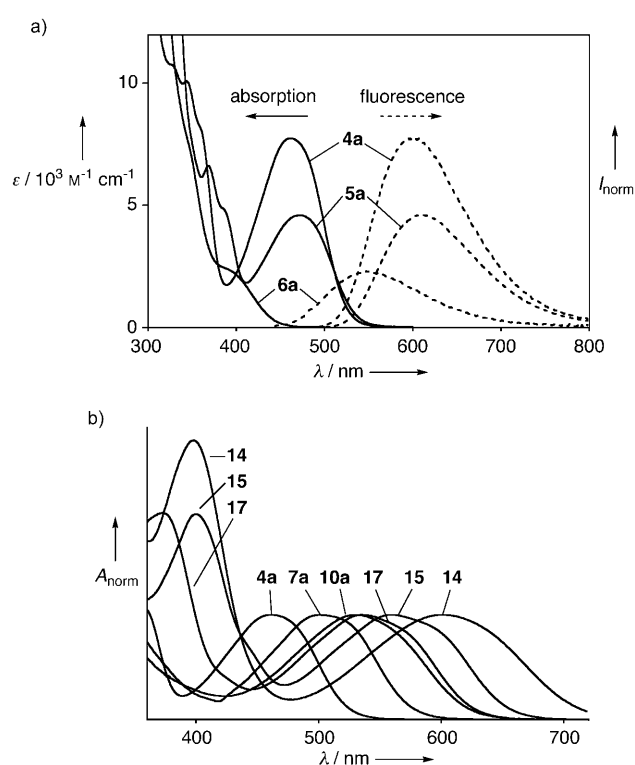

Figure 3. a) UV/Vis absorption and fluorescence spectra of **4a**, **5a**, and **6a** in CH$_2$Cl$_2$. b) UV/Vis absorption spectra (normalized) of **4a**, **7a**, **10a**, **14**, **15**, and **17** in CH$_2$Cl$_2$.

similar tendency was observed for a series of the 2-thienyl-substituted derivatives **4b–6b**, which show absorption and

Table 2. Optical and electrochemical data for bithiophene-fused benzo[c]phospholes.

	Absorption[a]		Fluorescence[a]		Stokes shift	Redox potentials[b]		
	λ_{abs} [nm][c]	ε [M^{-1}cm^{-1}]	λ_{em} [nm][d]	Φ_F [%][e]	[cm^{-1}]	E_{ox} [V][f]	E_{red} [V][f]	ΔE [V][g]
4a	462	7700	600	17.6	4980	0.45	−2.14	2.59
4b	483	8700	646	2.9	5220	0.36	−2.00	2.36
5a	472	4600	609	9.7	4770	0.47	−2.09	2.56
5b	491	4900	656	2.6	5120	0.39	−1.97	2.36
6a	395(sh)	2300	548	0.64	7070	0.66	−2.35	3.01
6b	409(sh)	3200	582	1.1	7270	0.56	−2.18	2.74
7a	502	5300	661	0.30	4790	0.83	−1.63	2.46
7b	535	6200	710	0.05	4610	0.66	−1.55	2.21
8a	503	2900	675	0.10	5070	0.86	−1.62	2.48
8b	539	3700	720	0.02	4660	0.70	−1.50	2.20
9a	420(sh)	1400	596	0.47	7030	1.12	−1.86	2.98
9b	435(sh)	2800	606	0.67	6490	0.88	−1.76	2.64
10a	530	4500	–	–	–	0.72[h]	−1.58	2.30
10b	566	5400	–	–	–	0.54	−1.45	1.99
11a	533	2400	–	–	–	0.78[h]	−1.54	2.32
11b	573	3000	–	–	–	0.59	−1.41	2.00
12a	427(sh)	1400	–	–	–	1.00	−1.80	2.80
13	544	6800	–	–	–	0.78	−1.45	2.23
14	603	7600	–	–	–	0.44	−1.50	1.94
15	561	9200	–	–	–	0.73	−1.43	2.16
16	473	15900	603	6.7	4560	0.55	−2.01	2.56
17	535	8000	–	–	–	0.83	−1.47	2.30

[a] Measured in CH$_2$Cl$_2$. [b] Determined by DPV in CH$_2$Cl$_2$ with 0.1 M nBu$_4$N$^+$PF$_6^-$. [c] The longest absorption maxima. [d] Excited at 440 nm for **4**, **5**, **7**, **8** and **16** and at 420 nm for **6** and **9**. [e] Fluorescence quantum yields determined by comparison with the reported value of Réau's 3,4-C$_4$-bridged 1-phenyl-2,5-bis(2-thienyl)phosphole–Au Complex ($\Phi_F=12.9$%; reference [4b]). [f] Redox potentials versus Fc/Fc$^+$ couple. [g] $E_{ox}-E_{red}$. [h] The second oxidation potentials of **10a** and **11a** are 0.83 V and 0.91 V, respectively.

emission maxima at longer wavelengths than do the phenyl-substituted derivatives **4a–6a** ($\Delta\lambda_{abs} = 14$–21 nm; $\Delta\lambda_{em} = 34$–47 nm: 2-thienyl versus phenyl). The Stokes shifts of **6a,b** (7070–7270 cm^{-1}) are considerably larger relative to those of **4a,b** (4980–5220 cm^{-1}) and **5a,b** (4770–5120 cm^{-1}). Evidently, the π-electrons in **6** are less efficiently delocalized over the fused rings than those in **4** and **5**, as all the three heterole rings are linked at the respective β-positions in **6**.

To further our understanding of the photodynamics of the three types of bithiophene-fused benzo[c]phospholes, we measured fluorescence lifetimes of **4a–6a** in CH$_2$Cl$_2$ at room temperature. The fluorescence decays were well-fitted by the single exponential component, and fluorescence lifetimes (τ_s) of **4a–6a** were determined to be 3.2, 4.1, and 0.18 ns, respectively. Note that τ_s value of the type-III compound (**6a**) is considerably smaller than τ_s values of type-I and type-II compounds (**4a** and **5a**). To shed light on nonradiative pathway from the S$_1$ state of these chromophores, we next evaluated the possibility of triplet formation of **4a–6a** in CH$_2$Cl$_2$ by the transient grating (TG) method.[23] The TG signals of the samples **4a** and **5a** showed only the thermal grating ones, which were built within a system response time (ca. 50 ns) and decayed by the thermal diffusion. On the other hand, the TG signal of the sample **6a** showed another slower buildup of the thermal grating signal (ca. 200 ns),[24] which was due to the nonradiative process from the triplet state produced by the intersystem crossing from the S$_1$ state. This slower rise component was amount to 80% of the total signal intensity. With these results in hand, we can safely conclude that the main pathway from the S$_1$ state of **6a** is not the direct relaxation to the S$_0$ state, but the intersystem crossing to the T$_1$ state. These results clearly show that the π-conjugation mode plays a crucial role in photodynamics of the bithiophene-fused benzo[c]phospholes.

It is known that chemical functionalizations at the phosphorus atom of phospholes change their optical properties dramatically.[1,2] In the present P,S-hybrid chromophores, the P-coordination to AuCl salt induces a bathochromic shift of the absorption and emission maxima ($\Delta\lambda_{abs} = 31$–52 nm and $\Delta\lambda_{em} = 61$–66 nm; for **7/8** versus **4/5**) and a considerable decrease in emission efficiency ($\Phi_F = 0.02$–1.1% for **7–9** versus $\Phi_F = 0.6$–17.6% for **4–6**). The oxygenation at the phosphorus atom causes more pronounced effects on the π–π* transitions, that is, the larger bathochromic shifts of absorption maxima ($\Delta\lambda_{abs} = 61$–83 nm for **10/11** versus **4/5**) and complete suppression of emission.

In the absorption spectra of **14**, **15**, and **17**, λ_{abs} of the lowest excitation bands were observed at 603, 561, and 535 nm, respectively. The bathochromic shift of λ_{abs} relative to that of the parent type-I P-oxide **10a** ($\lambda_{abs} = 530$ nm) is in the order: **14** ($\Delta\lambda_{abs} = 73$ nm) > **15** ($\Delta\lambda_{abs} = 31$ nm) > **17** ($\Delta\lambda_{abs} = 5$ nm). This indicates that the electron-donating aryl substituents at the bithiophene α,α′-positions narrow the HOMO–LUMO gap more significantly than the electron-withdrawing ones. It should be noted that **14**, **15**, and **17** exhibit other intense bands at $\lambda_{abs} = 398$, 400, and 373 nm, respectively, assignable to the π–π* transitions from HOMO

to LUMO+1 (vide infra). The above results demonstrate that the optical properties of bithiophene-fused benzo[c]-phospholes are also tunable by chemical modifications at the fused bithiophene backbone.

Electrochemical properties of bithiophene-fused benzo[c]-phospholes: Redox potentials of the bithiophene-fused benzo[c]phospholes were determined by means of cyclic voltammetry (CV) and differential pulse voltammetry (DPV). The measurement conditions are summarized in the caption of Table 2, and selected voltammograms are shown in Figure 4
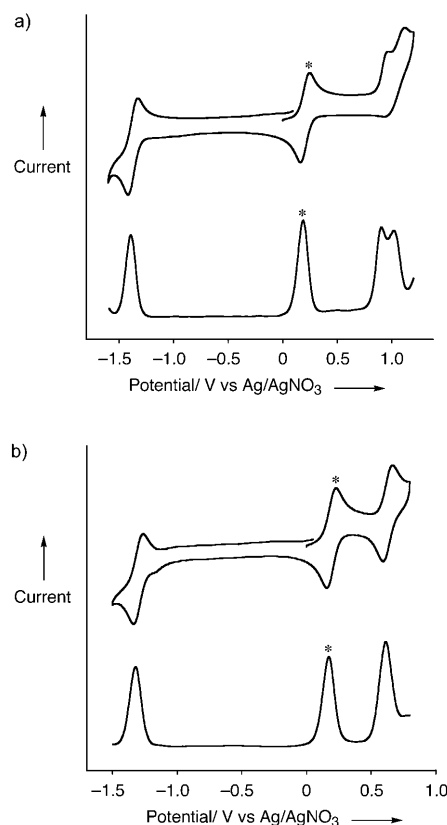
Figure 4. Cyclic voltammograms (upper) and differential pulse voltammograms (lower) of a) **10a** and b) **14**. Asterisks indicate Fc/Fc$^+$ couple.

and Figure S4 in the Supporting Information. The electrochemical oxidation and reduction processes of the σ^3-P derivatives **4–6** were found to be irreversible, and the redox potentials determined by DPV are listed in Table 2. The first oxidation potentials (E_{ox}) and the first reduction potentials (E_{red}) of the type-I compound **4a** ($E_{ox} = 0.45$ V; $E_{red} = -2.14$ V versus ferrocene/ferrocenium) and the type-II compound **5a** ($E_{ox} = 0.47$ V; $E_{red} = -2.09$ V) are comparable, which implies a subtle difference in their HOMO and LUMO energies. By contrast, the type-III compound **6a** showed more positive E_{ox} (0.66 V) and more negative E_{red} (−2.35 V), thus indicating that the HOMO–LUMO gap of **6a** ($\Delta E = 3.01$ V) is larger than that of **4a** ($\Delta E = 2.59$ V) and **5a** ($\Delta E = 2.56$ V). Replacing the 2,5-substituents at the

phosphole ring from phenyl to 2-thienyl shifted E_{ox} and E_{red} to the negative and positive directions, respectively, thereby narrowing the HOMO–LUMO gap by 0.20–0.34 V.

The chemical functionalizations at the phosphorus center explicitly affect the redox potentials of bithiophene-fused benzo[c]phospholes. The Au complexes **7–9** show irreversible voltammograms for oxidation and reduction processes at more positive side relative to those observed for the corresponding σ³-P compounds **4–6**. As was observed for Réau's phospholes **18** and **19**,[3c,4b] the coordination to AuCl salt lowers both HOMO and LUMO of the present P,S-hybrid π-systems. The reduction potentials of **10–12** are further shifted to the positive side ($\Delta E_{red} = 0.55$–0.58 V versus **4–6**) as compared to those of **7–9** ($\Delta E_{red} = 0.42$–0.51 V versus **4–6**), suggesting that the P-oxides are better electron acceptors than the P–Au complexes. It is likely that the σ*–π* orbital interaction between the phosphorus center and the P-linked diene unit becomes significant by the introduction of the oxo group (vide infra). Noticeably, **10–12** show reversible cyclic voltammograms for the reduction process as shown in Figure 4a and Figure S3, implying that the P-oxides are electrochemically stable in the one-electron reduction process.

The electronic effect of the π-conjugative heteroaryl substituents at the bithiophene moiety is also noteworthy. Introduction of 5-methyl-2-thienyl groups raises the HOMO level ($E_{ox} = 0.44$ V for **14** versus $E_{ox} = 0.72$ V for **10a**), whereas that of 2-thiazolyl groups lowers the LUMO level ($E_{ox} = -1.43$ V for **15** versus $E_{ox} = -1.58$ V for **10a**). As shown in Figure 4b, both oxidation and reduction processes of **14** occured reversibly. These results primarily reflect the electron-donating nature of the thienyl group and the electron-withdrawing nature of the thiazolyl group. The HOMO–LUMO gaps of **14** ($\Delta E = 1.94$ V) and **15** ($\Delta E = 2.16$ V) are smaller than the gap of **10a** ($\Delta E = 2.30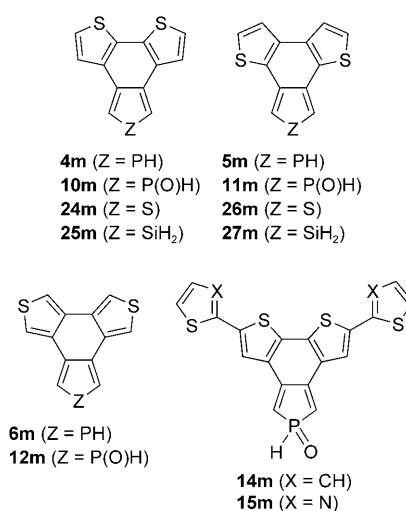$ V), implying that the π-networks at the bithiophene moiety in **14** and **15** are extended efficiently to the attached heteroaryl groups. The substitution with pentafluorophenyl groups does not change the HOMO–LUMO gap ($\Delta E = 2.30$ V for **17**), although both HOMO and LUMO levels are lowered in the same degree by the inductive effect. It is now evident that the character of frontier orbitals of bithiophene-fused benzo[c]phospholes is tunable by suitably modifying the α,α′-positions of the bithiophene subunit as well as the phosphorus center. The HOMO–LUMO gaps determined by electrochemical measurements are in good accordance with those estimated by UV/Vis absorption/emission spectra.

Theoretical studies on bithiophene-fused benzo[c]heteroles: To gain a deep insight into the electronic structures of bithiophene-fused benzo[c]phospholes and related benzo[c]-heteroles, we carried out DFT calculations of α-unsubstituted model compounds **4m–6m**, **10m–12m**, **14m**, **15m**, and **24m–27m**. The structures of these compounds were optimized at the B3LYP/6–31G* level, which is the same as that used for the theoretical calculation of unsubstituted benzo[c]phosphole.[11,25] The bond lengths and bond angles at the π-conjugated units of **4m**, **5m**, and **10m** are close to the

4m (Z = PH)
10m (Z = P(O)H)
24m (Z = S)
25m (Z = SiH₂)

5m (Z = PH)
11m (Z = P(O)H)
26m (Z = S)
27m (Z = SiH₂)

6m (Z = PH)
12m (Z = P(O)H)

14m (X = CH)
15m (X = N)

respective values of **4a**, **5a**, and **10a** determined by X-ray crystallography (Figure S4 in the Supporting Information). As visualized in Figure 5, the HOMO and the LUMO of each bithiophene-fused benzo[c]heterole basically consist of those derived from the heterole subunits. The HOMO of **4m** and **5m** holds antibonding character between the adjacent heterole rings, whereas the LUMO represents inter-ring bonding interactions. The calculated HOMO and LUMO energies (E_{HOMO} and E_{LUMO}) of the type-II model **5m** are close to those of the type-I model **4m** within 0.1 eV. In contrast, the HOMO and LUMO energies of **6m** are distinct from those of **4m** and **5m**. In particular, the LUMO of **6m** represents almost no inter-ring bonding interaction and is located at a much more positive level ($E_{LUMO} = -1.61$ eV) than that of **4m** ($E_{LUMO} = -1.93$ eV) and **5m** ($E_{LUMO} = -2.00$ eV). Consequently, the calculated HOMO–LUMO gap of **6m** ($\Delta E = 4.08$ eV) is considerably larger than that of **4m** ($\Delta E = 3.28$ eV) and **5m** ($\Delta E = 3.28$ eV).

As seen in Figure 5, the HOMO and LUMO energies of the P-oxo models **10m–12m** are lower by 0.40–0.42 eV and 0.78–0.81 eV, respectively, than those of the σ³-P models **4m–6m**. Hence, the HOMO–LUMO gaps of **10m–12m** become narrower by 0.36–0.41 eV relative to those of **4m–6m**. Evidently, the oxygenation at the phosphorus center stabilizes the LUMO more than the HOMO, due to the effective σ*–π* orbital interaction. The introduction of 2-thienyl and 2-thiazolyl groups at the α,α′-positions of the bithiophene subunit also perturbs the HOMO and LUMO energies. For example, replacement of the α-hydrogen atoms by the 2-thienyl groups (**10m–14m**) causes more pronounced effect on the HOMO ($E_{HOMO} = -5.63$ eV to -5.22 eV) than the LUMO ($E_{LUMO} = -2.71$ eV to -2.78 eV). The theoretically calculated substituent effects are in good accordance with the experimentally observed results (vide supra). Note that the LUMO+1 of **14m** and **15m**, the wavefunctions of which are extended to the heteroaryl substituents (Figure S5 in the Supporting Information), lie at -1.80 eV and -2.15 eV, respectively. The calculated HOMO–LUMO+1 gaps of **14m** and **15m** (3.42–

a)

24m
Z = S
R = H

4m
Z = PH
R = H

25m
Z = SiH$_2$
R = H

10m
Z = P(O)H
R = H

14m
Z = P(O)H
R = 2-thienyl

15m
Z = P(O)H
R = 2-thiazolyl

b)

26m
Z = S

5m
Z = PH

27m
Z = SiH$_2$

11m
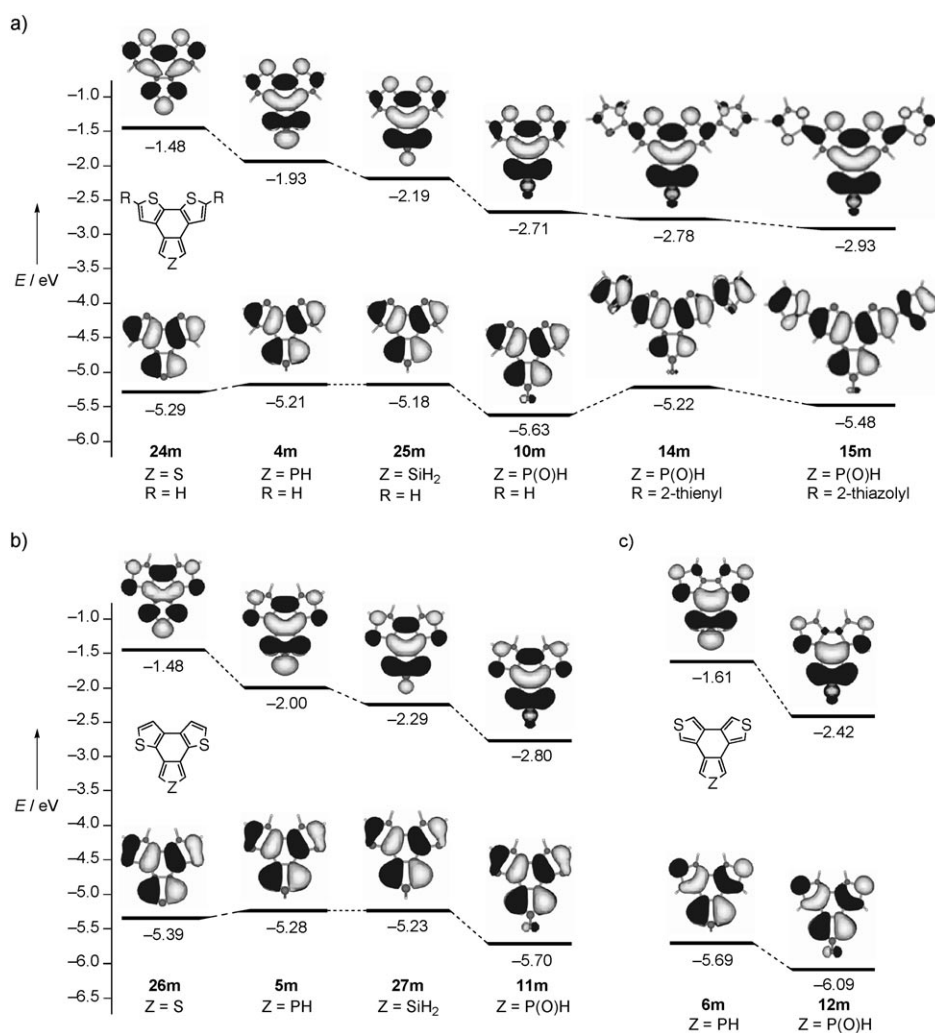Z = P(O)H

c)

6m
Z = PH

12m
Z = P(O)H

Figure 5. HOMO (lower) and LUMO (upper) of a) type-I bithiophene-fused benzo[c]heterole models **4m**, **10m**, **14m**, **15m**, **24m**, and **25m**, b) type-II models **5m**, **11m**, **26m**, and **27m**, and c) type-III models **6m** and **12m**. The orbital energies are given in eV.

3.33 eV) reasonably explain the appearance of the excitations at $\lambda_{abs} = 398$–400 nm in the UV/Vis spectra of **14** and **15** (Figure 3b).

To compare the electronic effects of heteroatoms on the frontier orbitals of bithiophene-fused benzo[c]heteroles, we also calculated benzo[c]thiophene models **24m** (type I) and **26m** (type II) and benzo[c]silole models **25m** (type I) and **27m** (type II) by using the same computational method. As shown in Figure 5, the HOMOs of **4m**, **24m**, and **25m** resemble one another, wherein the heteroatoms are on the node of orbitals. In fact, E_{HOMO} of **24m** and **25m** differ only slightly from E_{HOMO} of **4m** ($\Delta E_{HOMO} = -0.08$ to $+0.03$ eV). On the other hand, the LUMOs of **24m** and **25m** differ markedly from the LUMO of **4m** in shape and energy. That is, E_{LUMO} of benzo[c]thiophene **24m** is higher by 0.45 eV than that of **4m**, whereas E_{LUMO} of benzo[c]silole **25m** is lower by 0.26 eV than that of **4m**. The order of E_{LUMO} (**24m** > **4m** > **25m**) is in good agreement with that of the

corresponding heteroles (thiophene > σ^3-phosphole > silole),[1e] implying that the σ^*(E–H)–π^* orbital interaction (E = Si, P) intrinsically determines the LUMO levels of bithiophene-fused benzo[c]heteroles. It should be emphasized again that the making of the P-oxo bond stabilizes the LUMO more significantly than the HOMO due to the enhanced σ^*–π^* orbital interaction. Namely, E_{HOMO} and E_{LUMO} of **10m** are lower by 0.42 and 0.78 eV than E_{HOMO} and E_{LUMO} of **4m**, respectively. The calculated LUMO level of **10m** is lower than that of **25m**, suggesting the high electron-accepting ability of the P-oxo-benzo[c]phosphole π-network as compared to that of the benzo[c]silole π-network. A series of the type-II models **5m**, **11m**, **26m**, and **27m** exhibit almost the same tendency; the LUMO level lowers in the order: benzo[c]thiophene (**26m**) > σ^3-P-benzo[c]phosphole (**5m**) > benzo[c]silole (**27m**) > σ^4-P-benzo[c]phosphole (**11m**).

Electron mobility of a bithiophene-fused benzo[c]phosphole: As mentioned above, the P-oxo-type bithiophene-fused benzo[c]phospholes have been found to possess high electron-accepting ability. In addition, these P-oxides are reasonably stable in electrochemical reduction processes. Such properties are beneficial for designing efficient electron-transporting organic materials.[26] With this in mind, we conducted a time-of-flight (TOF) measurement to determine the electron mobility of **10a** as a representative example. The well-dried **10a** was deposited onto the surface of indium–tin–oxide (ITO) by sublimation in vacuo (0.5–0.7 nm s^{-1}; 10^{-3}–10^{-4} Pa). The device was once exposed to the atmosphere, and the aluminum electrode was made by vapor deposition (0.04 nm s^{-1}; 2.5–3.4 × 10^{-3} Pa). The thickness of the organic layer was 5.0 μm, which was determined by a stylus surface profiler (ULVAC Dektak 6M). The thickness of aluminum electrode was estimated to be ≈20 nm. Figure 6 depicts the field dependency of the logarithmic electron mobility of **10a**. The results of Alq$_3$ (film thickness = 5.3 μm), prepared and measured by the same vacuum deposition and TOF apparatuses in our
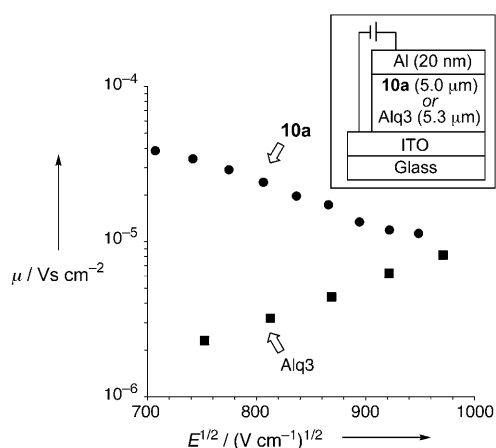
Figure 6. Electron mobilities (μ) of **10a** and Alq$_3$ versus square root of electric field (E). Circles: **10a**; squares: Alq$_3$ (measured in our lab). The inset shows a schematic image of the device used for the TOF measurement.

group, respectively, were also shown for reference. In sharp contrast to Alq$_3$, **10a** showed the negative field dependency of the electron mobility (μ), which increases with decreasing the electric field (E) and reaches the highest value ($\mu = 3.9 \times 10^{-5}$ cm^2 V^{-1} s^{-1}) at $E = 5.0 \times 10^5$ V cm^{-1}.[27] At the low electric fields, the mobilities of **10a** ($\mu = 2.9$–3.9×10^{-5} cm^2 V^{-1} s^{-1} at $E = 5.0$–6.0×10^5 V cm^{-1}) are about one-order higher than the mobility of Alq$_3$ ($\mu = 2.3 \times 10^{-6}$ cm^2 V^{-1} s^{-1} at $E = 5.7 \times 10^5$ V cm^{-1}).[28] This preliminary result suggests that the ring-fused benzo[c]phosphole oxides are promising candidates as the electron transporting materials.[29]

Conclusion

The Ti^{II}-mediated cyclization protocol has proven to be effective for the preparation of three types of bithiophene-fused benzo[c]phospholes, which are the first examples of thermally and kinetically stable benzo[c]phosphole. Both the experimental results (NMR spectroscopy, X-ray crystallography, absorption/emission spectroscopy, and CV/DPV) and the DFT computational results have revealed that the ring-fused pattern and the substituents at the heterole rings have a significant impact on the optical and electrochemical properties of bithiophene-fused benzo[c]phospholes. The appropriately fused σ^3-P derivatives and P–AuCl complexes are potential emitters with small HOMO–LUMO gaps covering the orange–red region, and the P-oxo derivatives are good electron acceptors with reasonable electrochemical stability. In addition, we have conducted the time-of-flight measurement to evaluate the electron mobility of the type-I P-oxo derivative, which exhibits high electron-transporting ability relative to Alq$_3$ at low electric fields. The present study demonstrates that the arene-fused benzo[c]phosphole skeleton could be a promising platform for the construction of a new class of phosphole-based π-conjugated materials in optoelectronic applications.

Experimental Section

General: All melting points are uncorrected. ^{1}H, ^{13}C{^{1}H} and ^{31}P{^{1}H} NMR spectra were recorded using CDCl$_3$ as the solvent unless otherwise noted. Chemical shifts are reported as the relative value versus tetramethylsilane (^{1}H and ^{13}C) and phosphoric acid (^{31}P). MALDI-TOF mass spectra were measured by using CHCA as a matrix. All solvents were distilled from sodium benzophenone ketyl (diethyl ether), or calcium hydride (CH$_2$Cl$_2$, toluene, Et$_3$N, iPr$_2$NH) before use. All the reactions were performed under an argon or nitrogen atmosphere. Column chromatography on silica gel was performed by using UltraPure Silicagel (230–400 mesh; SiliCycle), and thin-layer chromatography (TLC) was performed on silica gel 60 F254 (Merck). The reaction procedures for the synthesis of **1**–**9** and the ^{1}H NMR spectra of **4**–**9** were reported in the Supporting Information of reference [15]. In the present paper, the reaction procedures and spectral data for **10**–**17** are described.

Synthesis of 10a

Method A: m-CPBA (max 77%, 240 mg) was added to a solution of **4a** (470 mg, 1.0 mmol) in CH$_2$Cl$_2$ (30 mL). The color of the solution turned to purple in a few seconds, and the mixture was concentrated under reduced pressure. The solid residue was subjected to silica-gel column chromatography (CH$_2$Cl$_2$/acetone). The purple fraction was collected, evaporated, and reprecipitated from hexane/CH$_2$Cl$_2$ to give **10a** (460 mg, 94%) as a purple solid.

Method B: Alternatively, the crude mixture containing the corresponding σ^3-compound (prepared from **1a**, Ti(OiPr)$_4$, iPrMgCl, and PhPCl$_2$) was treated with m-CPBA. After column chromatography and reprecipitation, **10a** was obtained (Yield 63% from **1a**). M.p. 270°C (decomp); ^{1}H NMR (400 MHz, CD$_2$Cl$_2$): $\delta = 6.54$ (d, $J = 5.4$ Hz, 2H), 6.91 (d, $J = 5.4$ Hz, 2H), 6.9–7.5 (m, 10H), 7.43 (ddd, $J = 7.4$, 7.4 Hz, $^4J_{PH} = 2.8$ Hz, 2H), 7.47 (t, $J = 7.4$ Hz, 1H), 7.90 ppm (dd, $J = 7.4$, $^3J_{PH} = 12.2$ Hz, 2H); ^{13}C{^{1}H} NMR (100 MHz, CD$_2$Cl$_2$): $\delta = 123.8$, 126.9 (d, $J_{PC} = 94.6$ Hz), 127.3, 128.7 (d, $J_{PC} = 2.5$ Hz), 129.1 (br s), 129.4, 129.4 (d, $J_{PC} = 13.2$ Hz), 131.3, 131.6 (d, $J_{PC} = 93.0$ Hz), 131.6 (d, $J_{PC} = 9.9$ Hz), 132.7 (d, $J_{PC} = 2.5$ Hz), 134.1 (d, $J_{PC} = 8.2$ Hz), 137.6, 140.5 ppm (d, $J_{PC} = 29.6$ Hz); ^{31}P{^{1}H} NMR (162 MHz, CD$_2$Cl$_2$): $\delta = +37.8$ ppm; IR (KBr): $\tilde{\nu} = 1190$ cm^{-1} (P=O); MS (MALDI-TOF): m/z: 490 [M^+]; elemental analysis calcd (%) for C$_{30}$H$_{19}$OPS$_2$: C 73.45, H 3.90; found: C 73.29, H 3.63.

Synthesis of 10b: This compound was prepared from the corresponding σ^3-compound **4b** and m-CPBA according to a similar procedure (Method A) described for the synthesis of **10a**. Yield: 92%, purple solid; m.p. 275°C (decomp); ^{1}H NMR (400 MHz, CD$_2$Cl$_2$): $\delta = 6.94$ (d, $J = 5.4$ Hz, 2H), 7.00 (d, $J = 4.9$ Hz, 2H), 7.02 (d, $J = 5.4$ Hz, 2H), 7.06 (dd, $J = 4.9$, 4.9 Hz, 2H), 7.40 (d, $J = 4.9$ Hz, 2H), 7.45 (ddd, $J = 7.3$, 7.3 Hz, $^4J_{PH} = 2.8$ Hz, 2H), 7.57 (t, $J = 7.3$ Hz, 1H), 7.90 ppm (dd, $J = 7.3$, $^3J_{PH} = 12.2$ Hz, 2H); ^{13}C{^{1}H} NMR (75 MHz, CDCl$_3$): $\delta = 123.5$, 124.9 (d, $J_{PC} = 97.4$ Hz), 125.5 (d, $J_{PC} = 97.4$ Hz), 126.9, 127.7 (d, $J_{PC} = 1.9$ Hz), 127.8, 128.3 (d, $J_{PC} = 5.0$ Hz), 129.0 (d, $J_{PC} = 12.4$ Hz), 130.5 (d, $J_{PC} = 18.0$ Hz), 131.6 (d, $J_{PC} = 10.5$ Hz), 132.6 (d, $J_{PC} = 3.1$ Hz), 133.6 (d, $J_{PC} = 8.7$ Hz), 137.9, 141.5 ppm (d, $J_{PC} = 29.2$ Hz); ^{31}P{^{1}H} NMR (162 MHz, CDCl$_3$): $\delta = +35.8$ ppm; IR (KBr): $\tilde{\nu} = 1196$ cm^{-1} (P=O); MS (MALDI-TOF): m/z: 502 [M^+]; elemental analysis calcd (%) for C$_{26}$H$_{15}$OPS$_4$: C 62.13, H 3.01; found: C 62.25, H 3.13.

Synthesis of 11a: This compound was prepared from the corresponding σ^3-compound **5a** and m-CPBA according to a similar procedure (Method A) described for the synthesis of **10a**. Yield: 96%; wine red solid; m.p. >300°C; ^{1}H NMR (400 MHz, CD$_2$Cl$_2$): $\delta = 7.17$ (d, $J = 5.4$ Hz, 2H), 7.2–7.3 (m, 4H), 7.25 (d, $J = 5.4$ Hz, 2H), 7.35–7.4 (m, 6H), 7.44 (ddd, $J = 7.4$, 7.4 Hz, $^4J_{PH} = 2.9$ Hz, 2H), 7.56 (t, $J = 7.4$ Hz, 1H), 7.91 ppm (dd, $J = 7.4$, $^3J_{PH} = 12.2$ Hz, 2H); ^{13}C{^{1}H} NMR (100 MHz, CD$_2$Cl$_2$): $\delta = 123.4$, 126.7 (d, $J_{PC} = 96.3$ Hz), 129.1 (d, $J_{PC} = 1.6$ Hz), 129.3 (d, $J_{PC} = 4.1$ Hz), 129.5 (d, $J_{PC} = 11.5$ Hz), 129.6 (d, $J_{PC} = 1.6$ Hz), 130.4 (d, $J_{PC} = 95.5$ Hz), 130.6, 130.7, 131.7 (d, $J_{PC} = 9.9$ Hz), 132.7 (d, $J_{PC} = 2.5$ Hz), 133.0 (d, $J_{PC} = 8.2$ Hz), 137.9, 140.5 ppm (d, $J_{PC} = 30.5$ Hz); ^{31}P{^{1}H} NMR (162 MHz, CDCl$_3$): $\delta = +38.0$ ppm; IR (KBr): $\tilde{\nu} = 1200$ cm^{-1} (P=O); MS (MALDI-TOF): m/z: 490 [M^+]; elemental analysis calcd (%) for C$_{30}$H$_{19}$OPS$_2$: C 73.45, H 3.90; found: C 73.43, H 3.71.

Synthesis of 11 b: This compound was prepared from the corresponding σ^3-compound **5b** and *m*-CPBA according to a similar procedure (Method A) described for the synthesis of **10a**. Yield: 95%; purple solid; m.p. 270 °C (decomp); ^{1}H NMR (400 MHz, CD_2Cl_2): $\delta = 7.05–7.13$ (m, 4H), 7.22 (d, $J = 5.4$ Hz, 2H), 7.35 (d, $J = 5.4$ Hz, 2H), 7.4–7.5 (m, 4H), 7.59 (t, $J = 7.3$ Hz, 1H), 7.90 ppm (dd, $J = 7.3$, $^3J_{P,H} = 12.2$ Hz, 2H); $^{13}C\{^1H\}$ NMR (100 MHz, $CDCl_3$): $\delta = 123.0$, 124.1 (d, $J_{P,C} = 100.0$ Hz), 125.2 (d, $J_{P,C} = 99.2$ Hz), 128.0 (d, $J_{P,C} = 1.7$ Hz), 128.5 (d, $J_{P,C} = 2.5$ Hz), 128.7 (d, $J_{P,C} = 5.0$ Hz), 129.0 (d, $J_{P,C} = 12.4$ Hz), 129.8 (d, $J_{P,C} = 18.2$ Hz), 130.9, 131.6 (d, $J_{P,C} = 10.7$ Hz), 132.0 (d, $J_{P,C} = 9.1$ Hz), 132.7 (d, $J_{P,C} = 3.3$ Hz), 138.0, 141.9 ppm (d, $J_{P,C} = 30.6$ Hz); $^{31}P\{^1H\}$ NMR (162 MHz, $CDCl_3$): $\delta = +35.3$ ppm; IR (KBr): $\tilde{v} = 1200$ cm^{-1} (P=O); MS (MALDI-TOF): m/z: 502 [M^+]; elemental analysis calcd (%) for $C_{26}H_{15}OPS_4$: C 62.13, H 3.01; Found: C 62.12, H 3.08.

Synthesis of 12 a: This compound was prepared from the corresponding σ^3-compound **6a** and *m*-CPBA according to a similar procedure (Method A) described for the synthesis of **10a**. Yield: 94%; pale yellow solid; m.p. > 300 °C; ^{1}H NMR (400 MHz, CD_2Cl_2): $\delta = 7.05$ (d, $J = 2.9$ Hz, 2H), 7.1–7.45 (m, 10H), 7.44 (ddd, $J = 7.5$, 7.5 Hz, $^4J_{P,H} = 2.8$ Hz, 2H), 7.50 (d, $J = 2.9$ Hz, 2H), 7.53 (t, $J = 7.5$ Hz, 1H), 7.80 ppm (dd, $J = 7.5$, $^3J_{P,H} = 12.2$ Hz, 2H); $^{13}C\{^1H\}$ NMR (100 MHz, CD_2Cl_2): $\delta = 118.0$, 127.8 (d, $J_{P,C} = 98.0$ Hz), 127.9, 128.7 (d, $J_{P,C} = 1.7$ Hz), 129.3 (d, $J_{P,C} = 12.4$ Hz), 129.9, 130.6, 130.9 (d, $J_{P,C} = 96.7$ Hz), 131.6 (d, $J_{P,C} = 9.9$ Hz), 132.3, 132.5 (d, $J_{P,C} = 2.5$ Hz), 133.8, 134.5 (d, $J_{P,C} = 8.3$ Hz), 138.8 ppm (d, $J_{P,C} = 28.9$ Hz); $^{31}P\{^1H\}$ NMR (162 MHz, CD_2Cl_2): $\delta = +39.5$ ppm; IR (KBr): $\tilde{v} = 1195$ cm^{-1} (P=O); MS (MALDI-TOF): m/z: 490 [M^+]; elemental analysis calcd (%) for $C_{30}H_{19}OPS_2$: C 73.45, H 3.90; found: C 73.05, H 3.72.

Synthesis of 13: *n*BuLi (1.61 M × 1.37 mL, 2.2 mmol) was slowly added at −78 °C to a solution of **4a** (470 mg, 1.0 mmol) in THF (50 mL). The mixture was kept at this temperature for 20 min, and a solution of I_2 (640 mg, 2.5 mmol) in THF (5 mL) was added. The resulting mixture was slowly warmed to room temperature. After stirring for 2 h, the mixture was treated with saturated aq. $Na_2S_2O_3$ and extracted with CH_2Cl_2 twice. To the combined organic extracts was added *m*-CPBA (max 77%, 240 mg). The mixture was dried over Na_2SO_4, and concentrated under reduced pressure. The solid residue was subjected to silica-gel column chromatography (CH_2Cl_2/acetone). The purple fraction was collected, evaporated, and reprecipitated from diethyl ether/CH_2Cl_2 to give **13** (300 mg, 40%) as a purple solid. M.p. > 300 °C (decomp); ^{1}H NMR (400 MHz, CD_2Cl_2): $\delta = 6.66$ (s, 2H), 6.9–7.5 (m, 10H), 7.43 (ddd, $J = 7.4$, 7.4 Hz, $^4J_{P,H} = 2.9$ Hz, 2H), 7.55 (t, $J = 7.4$ Hz, 1H), 7.90 ppm (dd, $J = 7.4$, $^3J_{P,H} = 12.2$ Hz, 2H); $^{31}P\{^1H\}$ NMR (162 MHz, CD_2Cl_2): $\delta = +37.3$ ppm; IR (KBr): $\tilde{v} = 1187$ cm^{-1} (P=O); MS (MALDI-TOF): m/z: 742 [M^+]; elemental analysis calcd (%) for $C_{30}H_{17}I_2OPS_2$: C 48.54, H 2.31; found: C 48.70, H 2.31. ^{13}C NMR data could not be obtained due to low solubility.

Synthesis of 14: A mixture of **13** (74 mg, 0.10 mmol), 5-methyl-2-thiophene-boronic acid (31 mg, 0.22 mmol), [Pd(PPh$_3$)$_4$] (10 mg), K_3PO_4 (200 mg), and DMF (10 mL) was stirred for 3 h at 110 °C. Then water was added and the mixture was extracted with toluene several times. The combined organic extracts were washed with brine and dried over Na_2SO_4. After removal of the volatile components under reduced pressure, the residue was subjected to silica-gel column chromatography (CH_2Cl_2/acetone). The deep green fraction was collected, evaporated, and reprecipitated from MeOH to give **14** (21 mg, 31%) as a deep green solid. M.p. 290 °C (decomp); ^{1}H NMR (400 MHz, CD_2Cl_2): $\delta = 2.42$ (s, 6H), 6.46 (s, 2H), 6.62 (d, $J = 3.4$ Hz, 2H), 6.80 (d, $J = 3.4$ Hz, 2H), 6.9–7.5 (m, 10H), 7.45 (ddd, $J = 7.5$, 7.5 Hz, $^4J_{P,H} = 2.9$ Hz, 2H), 7.54 (t, $J = 7.5$ Hz, 1H), 7.93 ppm (dd, $J = 7.5$, $^3J_{P,H} = 12.2$ Hz, 2H); $^{31}P\{^1H\}$ NMR (162 MHz, CD_2Cl_2): $\delta = +37.4$ ppm; IR (KBr): $\tilde{v} = 1190$ cm^{-1} (P=O); MS (MALDI-TOF): m/z: 683 [M^+]; HRMS (FAB): m/z calcd for $C_{40}H_{27}OPS_4$: 682.0682; found: 682.0682. ^{13}C NMR data could not be obtained due to low solubility.

Synthesis of 15: A solution of 2-thiazolylzinc bromide in THF (ca. 0.5 M × 0.5 mL, prepared from 2-bromothiazole and activated zinc[30]) was added to a mixture of **13** (74 mg, 0.10 mmol), [Pd(PPh$_3$)$_4$] (10 mg), and THF (8 mL); the resulting mixture was heated under reflux for 7 h. Then water was added and the mixture was extracted with CH_2Cl_2 several

times. The combined organic extracts were washed with brine, and dried over Na_2SO_4. After removal of the volatile components under reduced pressure, the residue was subjected to silica-gel column chromatography (CH_2Cl_2/acetone). The purple fraction was collected, evaporated, and reprecipitated from MeOH to give **14** (13 mg, 20%) as a deep blue solid. M.p. 290 °C (decomp); ^{1}H NMR (400 MHz, CD_2Cl_2): $\delta = 6.87$ (s, 2H), 6.9–7.5 (m, 10H), 7.27 (d, $J = 3.4$ Hz, 2H), 7.46 (ddd, $J = 7.5$, 7.5 Hz, $^4J_{P,H} = 2.9$ Hz, 2H), 7.58 (t, $J = 7.5$ Hz, 1H), 7.72 (d, $J = 3.4$ Hz, 2H), 7.94 ppm (dd, $J = 7.5$, $^3J_{P,H} = 12.2$ Hz, 2H); $^{31}P\{^1H\}$ NMR (162 MHz, CD_2Cl_2): $\delta = +37.5$ ppm; IR (KBr): $\tilde{v} = 1195$ cm^{-1} (P=O); MS (MALDI-TOF): m/z: 657 [M^+]; HRMS (FAB): m/z calcd for $C_{36}H_{21}ON_2PS_4$: 656.0274; found: 656.0269 [M^+]. ^{13}C NMR data could not be obtained due to low solubility.

Synthesis of 16: *n*BuLi (1.61 M × 0.27 mL, 0.44 mmol) was slowly added at −78 °C to a solution of **4a** (95 mg, 0.20 mmol) in THF (10 mL). The mixture was kept at this temperature for 20 min, and hexafluorobenzene (0.40 mL) was added. The resulting mixture was slowly warmed to room temperature and stirred for 8 h. Then water was added and the mixture was extracted with CH_2Cl_2 several times. The combined organic extracts were washed with brine and dried over Na_2SO_4. After removal of the volatile components under reduced pressure, the residue was subjected to silica-gel column chromatography (CH_2Cl_2). The orange fraction was collected, evaporated, and reprecipitated from MeOH to give **16** (65 mg, 40%) as a reddish orange solid. M.p. 205 °C (decomp); ^{1}H NMR (400 MHz, CD_2Cl_2): $\delta = 7.1–7.3$ (m, 5H), 7.3–7.45 ppm (m, 12H); $^{13}C\{^1H\}$ NMR (100 MHz, CD_2Cl_2): $\delta = 124.6$ (m), 127.8, 127.9 (d, $J_{P,C} = 8.3$ Hz), 128.9 (d, $J_{P,C} = 12.4$ Hz), 129.0, 129.1 (d, $J_{P,C} = 9.1$ Hz), 129.7 (d, $J_{P,C} = 7.4$ Hz), 130.6 (d, $J_{P,C} = 2.5$ Hz), 133.5 (d, $J_{P,C} = 3.5$ Hz), 135.0 (d, $J_{P,C} = 21.7$ Hz), 135.0 (d, $J_{P,C} = 17.4$ Hz), 135.2 (d, $J_{P,C} = 3.0$ Hz), 137.4 (d, $J_{P,C} = 15.7$ Hz), 138.1 (dm, $J_{F,C} = 250$ Hz), 140.5 (dm, $J_{F,C} = 250$ Hz), 144.3 (dm, $J_{F,C} = 250$ Hz), 147.5 ppm (d, $J_{P,C} = 1.7$ Hz); $^{31}P\{^1H\}$ NMR (162 MHz, CD_2Cl_2): $\delta = +26.2$ ppm; MS (MALDI-TOF): m/z: 807 [M^+]; HRMS (FAB): m/z calcd for $C_{42}H_{17}F_{10}PS_2$: 806.0350; found: 806.0377 [M^+]. One of the carbon atoms could not be detected clearly in the ^{13}C NMR spectrum.

Synthesis of 17: This compound was prepared from the corresponding σ^3-compound **16** and *m*-CPBA according to a similar procedure (Method A) described above for the synthesis of **10a**. Yield: 92%, purple solid; m.p. 300 °C (decomp); ^{1}H NMR (400 MHz, CD_2Cl_2): $\delta = 7.08$ (s, 2H), 7.0–7.5 (m, 10H), 7.46 (ddd, $J = 7.4$, 7.4 Hz, $^4J_{P,H} = 2.9$ Hz, 2H), 7.57 (t, $J = 7.4$ Hz, 1H), 7.92 ppm (dd, $J = 7.4$, $^3J_{P,H} = 12.2$ Hz, 2H); $^{13}C\{^1H\}$ NMR (100 MHz, CD_2Cl_2): $\delta = 109.1$ (m), 125.0, 125.6 (br s), 126.4 (d, $J_{P,C} = 95.1$ Hz), 128.9 (br s), 129.1 (d, $J_{P,C} = 1.7$ Hz), 129.6, 129.6 (d, $J_{P,C} = 12.4$ Hz), 131.6 (d, $J_{P,C} = 10.7$ Hz), 132.1, 132.2 (d, $J_{P,C} = 73.6$ Hz), 132.9 (d, $J_{P,C} = 2.5$ Hz), 133.5 (d, $J_{P,C} = 8.3$ Hz), 138.0, 138.3 (dm, $J_{F,C} = 250$ Hz), 139.3 (d, $J_{P,C} = 29.8$ Hz), 140.9 (dm, $J_{F,C} = 250$ Hz), 144.4 ppm (dm, $J_{F,C} = 250$ Hz); $^{31}P\{^1H\}$ NMR (162 MHz, CD_2Cl_2): $\delta = +37.9$ ppm; IR (KBr): $\tilde{v} = 1192$ cm^{-1} (P=O); MS (MALDI-TOF): m/z: 823 [M^+]; HRMS (FAB): m/z calcd for $C_{42}H_{17}OF_{10}PS_2$: 822.0299; found: 822.0284 [M^+].

X-ray crystal crystallographic analysis: Single crystals were grown from CH_2Cl_2–MeOH (for **4a**, **5a**, **7a**, **8a**, and **9a**) or CH_2Cl_2–hexane (for **10a**) at room temperature. All measurements were made on a Rigaku Saturn CCD area detector with graphite monochromated Mo$_{K\alpha}$ radiation ($\lambda = 0.71069$ Å). The structures were solved by direct methods,[31] and expanded using Fourier techniques.[32] Non-hydrogen atoms were refined anisotropically, and hydrogen atoms were refined by using the rigid model. All calculations were performed using CrystalStructure crystallographic software package[33] except for refinement, which was performed using SHELXL-97.[34] The structural parameters are summarized in Table 3. CCDC-660029 (**4a**), CCDC-687636 (**5a**), CCDC-660028 (**7a**), CCDC-687637 (**8a**), CCDC-687635 (**9a**), and CCDC-687638 (**10a**) contain the supplementary crystallographic data for this paper. These data can be obtained free of charge from The Cambridge Crystallographic Data Centre via www.ccdc.cam.ac.uk/data_request/cif.

Fluorescence lifetime and transient-grating measurements: The fluorescence lifetime was measured in CH_2Cl_2 by using a streak camera as a fluorescence detector. Samples **4a** and **5a** were excited by the 480 nm laser pulse produced by an optical parametric amplification system oper-

FULL PAPER

Table 3. X-ray structural parameters of **4a**, **5a**, **7a**, **8a**, **9a**, and **10a**.

	4a	5a	7a	8a	9a	10a
formula	$C_{30}H_{19}PS_2$	$C_{30}H_{19}PS_2$	$C_{31}H_{21}AuCl_3PS_2$	$C_{30}H_{19}AuClPS_2$	$C_{30}H_{19}AuClPS_2$	$C_{30}H_{19}OPS_2$
formula weight	474.54	474.54	791.88	706.96	706.96	490.54
crystal size (mm)	$0.45 \times 0.20 \times 0.15$	$0.25 \times 0.20 \times 0.10$	$0.20 \times 0.15 \times 0.05$	$0.30 \times 0.20 \times 0.03$	$0.20 \times 0.15 \times 0.04$	$0.30 \times 0.15 \times 0.05$
crystal system	monoclininc	triclinic	triclinic	monoclininc	monoclinic	triclinic
a [Å]	6.2062(2)	9.930(2)	9.888(3)	19.210(3)	19.141(3)	10.044(8)
b [Å]	21.4229(9)	10.098(2)	12.243(4)	13.1441(18)	13.200(2)	10.278(8)
c [Å]	17.4039(8)	12.819(3)	12.481(4)	21.304(3)	21.155(3)	12.845(9)
α [°]	90	85.808(9)	100.709(4)	90	90	93.010(9)
β [°]	97.372(3)	87.573(10)	102.781(4)	102.890(2)	102.716(2)	98.884(4)
γ [°]	90	63.481(5)	95.077(4)	90	90	116.591(9)
V [Å³]	2294.80(16)	1147.0(4)	1434.5(8)	5243.6(13)	5214.1(14)	1160.4(15)
space group	$P2_1/n$	$P\bar{1}$	$P\bar{1}$	$P2_1/a$	$P2_1/a$	$P\bar{1}$
Z	4	2	2	8	8	2
ρ_{calcd} [g cm^{-3}]	1.374	1.374	1.833	1.791	1.801	1.404
μ [cm^{-1}]	3.19	3.19	56.29	59.51	59.85	3.21
T [°C]	−150	−150	−150	−150	−150	−150
$2\theta_{max}$ [°]	55.0	55.0	55.0	55.0	55.0	55.0
independent reflns	5203	4980	6302	11 949	11 595	5089
variables	299	299	344	632	632	308
R [$I > 2.00\sigma(I)$]	0.0383	0.0440	0.0329	0.0427	0.0699	0.0829
wR (all)	0.0752	0.0896	0.0678	0.0959	0.1218	0.1575
goodness of fit	1.015	1.034	1.012	1.009	1.066	1.052

ated by the output from an amplified femto-second Ti:Sapphire laser system. Sample **6a** was excited by the second harmonic output (400 nm) from the same Ti:Sapphire laser system.

The production of the triplet state was confirmed by the transient grating measurement. The experimental setup was almost the same as that in reference [23] except for the excitation wavelength (442 nm). The TG signal was monitored by the 633 nm CW laser. Before the TG measurement, the sample solution (CH$_2$Cl$_2$) was bubbled by argon gas for more than 10 min to remove oxygen dissolved in the solution.

Electrochemical measurements: These were performed in CH$_2$Cl$_2$ with a glassy carbon working electrode, a platinum wire counter electrode, and an Ag/Ag$^+$ [0.01 M AgNO$_3$, 0.1 M nBu$_4$NPF$_6$ (MeCN)] reference electrode. The potentials were calibrated with ferrocene/ferrocenium as an internal standard.

Density functional theory (DFT) calculations: All calculations were performed using the Gaussian 03[35] suite of programs with the 6-31G* basis set[36] and the B3LYP functional.[37] The geometries were fully optimized without any symmetry constraints. The molecular orbital diagrams were drawn using MolStudio R3.0 (NEC Corp., Japan).

Time-of-flight measurement for 10a: Time-of-flight measurements were carried out at room temperature on a Sumitomo Heavy Industries Advanced Machinery (Optel) TOF-401 equipment.

Acknowledgement

[1] For reviews, see: a) L. D. Quin, *The Heterocyclic Chemistry of Phosphorus*, Wiley, New York, **1981**; b) F. Mathey, *Chem. Rev.* **1988**, *88*, 429–453; c) L. D. Quin, in *Comprehensive Heterocyclic Chemistry, Vol. 2* (Eds.: A. R. Katritzky, C. W. Rees, E. F. V. Scriven), Elsevier, Oxford, **1996**; d) F. Mathey, *Phosphorus–Carbon Heterocyclic Chemistry: The Rise of a New Domain*, Elsevier, Oxford, **2001**; e) L. Nyulászi, *Chem. Rev.* **2001**, *101*, 1229–1246; f) F. Mathey, *Angew. Chem.* **2003**, *115*, 1616–1643; *Angew. Chem. Int. Ed.* **2003**, *42*, 1578–1604; g) L. D. Quin, *Curr. Org. Chem.* **2006**, *10*, 43–78.

[2] For reviews, see: a) M. Hissler, P. W. Dyer, R. Réau, *Coord. Chem. Rev.* **2003**, *244*, 1–44; b) T. Baumgartner, R. Réau, *Chem. Rev.* **2006**, *106*, 4681–4727 (corrigendum: T. Baumgartner, R. Réau, *Chem. Rev.* **2007**, *107*, 303); c) P. W. Dyer, R. Réau, in *Functional Organic Materials* (Eds.: T. J. J. Müller, U. H. F. Bunz), Wiley-VCH, Weinheim, **2007**, pp. 119–177; d) M. Hissler, C. Lescop, R. Réau, *C. R. Chim.* **2008**, *11*, 628–640; e) M. G. Hobbs, T. Baumgartner, *Eur. J. Inorg. Chem.* **2007**, 3611–3628.

[3] a) C. Hay, D. L. Vilain, V. Deborde, L. Toupet, R. Réau, *Chem. Commun.* **1999**, 345–346; b) C. Hay, C. Fischmeister, M. Hissler, L. Toupet, R. Réau, *Angew. Chem.* **2000**, *112*, 1882–1885; *Angew. Chem. Int. Ed.* **2000**, *39*, 1812–1815; c) C. Hay, C. Fischmeister, J. Rault-Berthelot, L. Toupet, L. Nyulászi, R. Réau, *Chem. Eur. J.* **2001**, *7*, 4222–4236; d) C. Hay, C. Fave, M. Hissler, J. Rault-Berthelot, R. Réau, *Org. Lett.* **2003**, *5*, 3467–3470; e) C. Fave, M. Hissler, T. Kárpáti, J. Rault-Berthelot, V. Deborde, L. Toupet, L. Nyulászi, R. Réau, *J. Am. Chem. Soc.* **2004**, *126*, 6058–6063; f) B. Nohra, S. Graule, C. Lescop, R. Réau, *J. Am. Chem. Soc.* **2006**, *128*, 3520–3521; see also references [2a–d].

[4] a) C. Fave, T.-Y. Cho, M. Hissler, C.-W. Chen, T.-Y. Luh, C.-C. Wu, R. Réau, *J. Am. Chem. Soc.* **2003**, *125*, 9254–9255; b) H.-C. Su, O. Fedhel, C.-J. Yang, T.-Y. Cho, C. Fave, M. Hissler, C.-C. Wu, R. Réau, *J. Am. Chem. Soc.* **2006**, *128*, 983–995.

[5] a) M.-O. Bévierre, F. Mercier, F. Mathey, A. Jutand, C. Amatore, *New J. Chem.* **1991**, *15*, 545–550; b) S. S. H. Mao, T. D. Tilley, *Macromolecules* **1997**, *30*, 5566–5569; c) Y. Morisaki, Y. Aiki, Y. Chujo, *Macromolecules* **2003**, *36*, 2594–2597; d) I. Tomita, M. Ueda, *Macromol. Symp.* **2004**, *209*, 217–230; e) T. Sanji, K. Shiraishi, M. Tanaka, *Org. Lett.* **2007**, *9*, 3611–3614; f) H.-S. Na, Y. Morisaki, Y. Aiki, Y. Chujo, *Polym. Bull.* **2007**, *58*, 645–652; g) H.-S. Na, Y. Morisaki, Y. Aiki, Y. Chujo, *J. Polym. Sci. Part A* **2007**, *45*, 2867–2875.

[6] a) C. Fave, M. Hissler, K. Sénéchal, I. Ledoux, J. Zyss, R. Réau, *Chem. Commun.* **2002**, 1674–1675; b) Y. Matano, T. Miyajima, H. Imahori, Y. Kimura, *J. Org. Chem.* **2007**, *72*, 6200–6205.

[7] a) D. Delaere, M. T. Nguyen, L. G. Vanquickenborne, *Phys. Chem. Chem. Phys.* **2002**, *4*, 1522–1530; b) D. Delaere, M. T. Nguyen, L. G. Vanquickenborne, *J. Phys. Chem. A* **2003**, *107*, 838–846; c) Y.-L. Liu, J.-K. Feng, A.-M. Ren, *J. Comput. Chem.* **2007**, *28*, 2500–2509;

d) G. Zhang, J. Ma, J. Wen, *J. Phys. Chem. B* **2007**, *111*, 11670–11679.

[8] a) S. Kobayashi, M. Noguchi, Y. Tsubata, M. Kitano, H. Doi, T. Kamioka, A. Nakazono, Jpn. Pat. 2003231741, **2003**; b) Y. Makioka, T. Hayashi, M. Tanaka, *Chem. Lett.* **2004**, *33*, 44–45; see also reference [4b].

[9] a) T. Baumgartner, *Macromol. Symp.* **2003**, *196*, 279–288; b) T. Baumgartner, T. Neumann, B. Wirges, *Angew. Chem.* **2004**, *116*, 6323–6328; *Angew. Chem. Int. Ed.* **2004**, *43*, 6197–6201; c) T. Baumgartner, W. Bergmans, T. Kárpáti, T. Neumann, M. Nieger, L. Nyulázi, *Chem. Eur. J.* **2005**, *11*, 4687–4699; d) Y. Dienes, S. Durben, T. Kárpáti, T. Neumann, U. Englert, L. Nyulázi, T. Baumgartner, *Chem. Eur. J.* **2007**, *13*, 7487–7500; e) A. Acharya, Y. Koizumi, S. Seki, A. Saeki, S. Tagawa, Y. Ie, Y. Aso, *J. Photochem. Photobiol. A* **2005**, *173*, 161–168.

[10] A. Fukazawa, M. Hara, T. Okamoto, E.-C. Son, C. Xu, K. Tamao, S. Yamaguchi, *Org. Lett.* **2008**, *10*, 913–916.

[11] T. C. Dinadayalane, G. N. Sastry, *J. Chem. Soc. Perkin Trans. 2* **2002**, 1902–1908.

[12] R.-F. Chen, C. Zheng, Q.-L. Fan, W. Huang, *J. Comput. Chem.* **2007**, *28*, 2091–2101. The calculated dibenzo[*b,d*]phospholes bear phenyl or methyl group at the phosphorus center. In this study, we determined the HOMO and LUMO energies of unsubstituted dibenzo-[*b,d*]phosphole at the B3LYP/6-31G* level as −6.00 and −1.00 eV, respectively.

[13] a) J. M. Holland, D. W. Jones, *J. Chem. Soc. Chem. Commun.* **1970**, 122; b) J. M. Holland, D. W. Jones, *J. Chem. Soc. Perkin Trans. 1* **1973**, 927–931; c) T. H. Chan, K. T. Nwe, *Tetrahedron Lett.* **1973**, *14*, 4815–4818; d) T. H. Chan, K. T. Nwe, *Tetrahedron* **1975**, *31*, 2537–2542; e) A. Decken, F. Bottomley, B. E. Wilkins, E. D. Gill, *Organometallics* **2004**, *23*, 3683–3693; f) R. A. Aitken, in *Science of Synthesis, Vol. 10* (Eds.: D. Bellus, S. V. Ley, R. Noyori, M. Regitz, P. J. Reider, E. Schaumann, I. Shinkai, E. J. Thomas, B. M. Trost), Thieme, New York, **2000**, pp. 809–815.

[14] A benzo[*c*]phosphole bearing triphenylphosphonio groups at the 2,5-positions was isolated as a highly moisture-sensitive solid, although its fundamental properties have not been reported. See: A. Schmidpeter, M. Thiele, *Angew. Chem.* **1991**, *103*, 333–335; *Angew. Chem. Int. Ed. Engl.* **1991**, *30*, 308–310.

[15] Preliminary results were reported as a Communication. See: T. Miyajima, Y. Matano, H. Imahori, *Eur. J. Org. Chem.* **2008**, 255–259.

[16] For the syntheses of phospholes via titanacyclopentadienes, see: a) I. Tomita, *Polym. Prepr.* **2004**, *45*, 415–416; b) Y. Matano, T. Miyajima, T. Nakabuchi, Y. Matsutani, H. Imahori, *J. Org. Chem.* **2006**, *71*, 5792–5795; see also references [5d,e], [6b], and [15].

[17] U. Dahlmann, R. Neidlein, *Helv. Chim. Acta* **1996**, *79*, 755–766.

[18] a) H. Urabe, T. Hata, F. Sato, *Tetrahedron Lett.* **1995**, *36*, 4261–4264; b) H. Urabe, F. Sato, *J. Org. Chem.* **1996**, *61*, 6756–6757; c) F. Sato, H. Urabe, S. Okamoto, *Chem. Rev.* **2000**, *100*, 2835–2886; d) K. Mikami, Y. Matsumoto, T. Shiono, in *Science of Synthesis, Vol. 2* (Eds.: D. Bellus, S. V. Ley, R. Noyori, M. Regitz, P. J. Reider, E. Schaumann, I. Shinkai, E. J. Thomas, B. M. Trost), Thieme, New York, **2003**, pp. 809–815, and references therein.

[19] In single crystals of **8a** and **9a**, one dichloromethane molecule was incorporated per two benzo[*c*]phosphole molecules, whose structures are very similar. Therefore, the data for one of the pair are listed for **8a** and **9a** in Table 1.

[20] a) S. Attar, W. H. Bearden, N. W. Alcock, E. C. Alyea, J. H. Nelson, *Inorg. Chem.* **1990**, *29*, 425–433; Au−P, 2.220(9)–2.227(2) Å; P-Au-Cl, 172.4(1)–178.8(1)°; b) See refernce [4b]; Au−P, 2.2290(16)–2.2300(16) Å; P-Au-Cl, 171.64(7)–174.63(8)°; c) Y. Dienes, M. Eggenstein, T. Neumann, U. Englert, T. Baumgartner, *Dalton Trans.* **2006**, 1424–1433; Au−P, 2.2249(12) Å; P-Au-Cl, 177.26(4)°; Au−P, 2.228(2) Å; P-Au-Cl, 177.26(4)°; d) see reference [9c]; Au−P, 2.228(2) Å; P-Au-Cl, 175.59(7)°.

[21] The π–π distances between two planes in **7a**, **8a**, and **9a** are about 3.4–3.6 Å.

[22] The electronic factor, namely dipole-dipole interaction of the adjacent chromophores, may also assist the head-to-head orientation of **7a**, **8a**, and **9a**.

[23] For details, see: M. Terazima, N. Hirota, *J. Chem. Phys.* **1991**, *95*, 6490–6495.

[24] The slower rise component was quenched by the addition of oxygen into the solution.

[25] In our preliminary communication, we reported the optimized structures of P-phenyl analogues of **4m**–**6m**, whose HOMO and LUMO energies are as follows: **4m**–**Ph** (−5.10 eV and −1.89 eV), **5m**–**Ph** (−5.16 and −1.96 eV), **6m**–**Ph** (−5.55 and −1.60 eV). See reference [15].

[26] There are some reports on OLEDs using triorganylphosphine oxides as the component of electron transporting layers. For example, see: a) P. E. Burrows, A. B. Padmaperuma, L. S. Sapochak, P. Djurovich, M. E. Thompson, *Appl. Phys. Lett.* **2006**, *88*, 183503; b) A. B. Padmaperuma, L. S. Sapochak, P. E. Burrows, *Chem. Mater.* **2006**, *18*, 2389–2396; c) T. Oyamada, H. Sasabe, C. Adachi, S. Murase, T. Tominaga, C. Maeda, *Appl. Phys. Lett.* **2005**, *86*, 033503; d) T. Matsushima, C. Adachi, *Appl. Phys. Lett.* **2006**, *89*, 253506; e) N. Rehmann, D. Hertel, K. Meerholz, H. Becker, S. Heun, *Appl. Phys. Lett.* **2007**, *91*, 103507.

[27] The negative field dependency of the mobility has been observed for several hole/electron-transporting materials. For example, see: "Organic Photoreceptors for Xerography" P. M. Borsenberger, D. S. Weiss, *Optical Engineering Vol. 59* (Ed.: B. J. Thompson), Marcel Dekker, New York, **1998**, pp. 300–305.

[28] The electron mobilities of Alq₃ reported by Naka and co-workers are about 2.5 times larger than our experimental values. See: a) S. Naka, H. Okada, H. Onnagawa, T. Tsutsui, *Appl. Phys. Lett.* **2000**, *76*, 197–199; b) S. Naka, H. Okada, H. Onnagawa, Y. Yamaguchi, T. Tsutsui, *Synth. Met.* **2000**, *111–112*, 331–333.

[29] During the preparation of our manuscript, Tsuji, Nakamura, and co-workers reported the electron mobility of a benzo[*b*]phosphole oxide by the TOF technique using a vacuum-deposited film. See: H. Tsuji, K. Sato, L. Ilies, Y. Itoh, Y. Sato, E. Nakamura, *Org. Lett.* **2008**, *10*, 2263–2265.

[30] A. S. B. Prasad, T. M. Stevenson, J. R. Citineni, V. Nyzam, P. Knochel, *Tetrahedron* **1997**, *53*, 7237–7254.

[31] A. Altomare, G. Cascarano, C. Giacovazzo, A. Guagliardi, M. Burla, G. Polidori, M. Camalli, *J. Appl. Crystallogr.* **1994**, *27*, 435.

[32] DIRDIF99: Beurskens, P. T., Admiraal, G., Beurskens, W. P. Bosman, R. de Gelder, R. Israel, J. M. M. Smits, The DIRDIF-99 program system, Technical Report of the Crystallography Laboratory, University of Nijmegen (The Netherlands), **1999**.

[33] CrystalStructure 3.8.0: Crystal Structure Analysis Package, Rigaku and Rigaku/MSC (2000–2006). 9009 New Trails Dr. The Woodlands, TX 77381, USA.

[34] G. M. Sheldrick, *SHELXL-97*, University of Göttingen (Germany), **1997**.

[35] M. J. Frisch, G. W. Trucks, H. B. Schlegel, G. E. Scuseria, M. A. Robb, J. R. Cheeseman, J. A. Montgomery, Jr., T. Vreven, K. N. Kudin, J. C. Burant, J. M. Millam, S. S. Iyengar, J. Tomasi, V. Barone, B. Mennucci, M. Cossi, G. Scalmani, N. Rega, G. A. Petersson, H. Nakatsuji, M. Hada, M. Ehara, K. Toyota, R. Fukuda, J. Hasegawa, M. Ishida, T. Nakajima, Y. Honda, O. Kitao, H. Nakai, M. Klene, X. Li, J. E. Knox, H. P. Hratchian, J. B. Cross, C. Adamo, J. Jaramillo, R. Gomperts, R. E. Stratmann, O. Yazyev, A. J. Austin, R. Cammi, C. Pomelli, J. W. Ochterski, P. Y. Ayala, K. Morokuma, G. A. Voth, P. Salvador, J. J. Dannenberg, V. G. Zakrzewski, S. Dapprich, A. D. Daniels, M. C. Strain, O. Farkas, D. K. Malick, A. D. Rabuck, K. Raghavachari, J. B. Foresman, J. V. Ortiz, Q. Cui, A. G. Baboul, S. Clifford, J. Cioslowski, B. B. Stefanov, G. Liu, A. Liashenko, P. Piskorz, I. Komaromi, R. L. Martin, D. J. Fox, T. Keith, M. A. Al-Laham, C. Y. Peng, A. Nanayakkara, M. Challacombe, P. M. W. Gill, B. Johnson, W. Chen, M. W. Wong, C. Gonzalez, J. A. Pople, Gaussian 03, Gaussian, Pittsburgh, PA, **2003**.

[36] a) W. J. Hehre, R. Ditchfield, J. A. Pople, *J. Chem. Phys.* **1972**, *56*, 2257–2261; b) M. M. Francl, W. J. Pietro, W. J. Hehre, J. S. Binkley,

M. S. Gordon, D. J. DeFrees, J. A. Pople, *J. Chem. Phys.* **1982**, *77*, 3654–3665.

[37] a) A. D. Becke, *Phys. Rev. A.* **1988**, *38*, 3098–3100; b) A. D. Becke, *J. Chem. Phys.* **1993**, *98*, 5648–5652; c) C. Lee, W. Yang, R. G. Parr, *Phys. Rev. B* **1988**, *37*, 785–789.